JOURNAL OF COMPUTATIONAL PHYSICS 76, 33–47 (1988)

The Interaction between a Compliant Material and an Unstable Boundary Layer Flow*

M. S. HALL

Lawrence Livermore National Laboratory, University of California Livermore, California 94550

Received November 20, 1986, revised June 29, 1987

The response of a compliant coating to pressure fluctuations due to an unsteady boundary layer flow and the effect of the response on the stability of the flow field are examined A pseudospectral solution of the Navier–Stokes equations is coupled to a finite element calculation of the behavior of the compliant material In particular, the effect of material response on the growth rate of a Tollmien–Schlichting type instability in an unstable boundary layer is examined Results are presented for three materials, a soft polyvinylchloride (PVC), a stiffer PVC, and a two-layer material consisting of a thick layer of soft PVC covered by a thin layer of neoprene

INTRODUCTION

A numerical method for studying the interaction between an unstable boundary layer flow and a compliant surface is considered here Since Kramer first demonstrated a reduction in the skin-friction drag on an underwater vessel due to interaction of the surrounding fluid with a compliant coating, this interaction has been investigated theoretically, experimentally, and computationally. Originally inspired by observations of the swimming efficiency of dolphins [1, 2], Kramer's experiments [3–5] did indeed result in significant reduction of the drag on towed cylinders. Two possible mechanisms for this reduction in drag have since been suggested. The compliant material might interact with a fully developed turbulent boundary layer in such a way as to reduce the intensity of the turbulence, or the material might interact with a laminar boundary layer in such a way as to delay the transition to turbulence

To date, most of the experimental work has focused on the turbulent interaction, with primarily negative results. This is true of studies done using coatings similar to those developed by Kramer [6–9] as well as studies done using simpler single or double-layer coatings [10–14]. A review of the experimental work prior to 1984 has been presented by Gad-el-Hak *et al.* [11] and in the paper by Carpenter and

* This work was performed under the auspices of the U S Department of Energy by Lawrence Livermore National Laboratory under Contract W-7405-ENG-48 and supported by the Department of the Navy, Office of Naval Research under Contract N000-14-83-F-0010

0021-9991/88 $3 00

Garrad [15], which contains a further discussion of Kramer's experiments and of attempts to duplicate Kramer's experiments.

Much of the numerical work that has been done has also focused on the interaction between a compliant coating and a fully developed turbulent flow. These investigations have included both noninteractive studies of material response, and quasi-interactive attempts to anticipate the response of a membrane or Voigt solid and couple the resulting velocities back into the flow field. Buckingham *et al.* [16] calculated the response of a variety of materials to Monte-Carlo generated random pressure fields, without considering the effect of the resultant interface displacements and velocities on the flow field. This work, which makes use of a turbulent wall pressure model developed by Ash [17] and Ash and Khorrami [18], provides a numerical counterpart to the theory first published by Phillips [19] on the generation of water waves by a random pressure fluctuation. Such an approach has two advantages: complex multi-layered and internally structured coatings can be characterized in terms of amplitude and frequency response, and flow-induced pressures are not restricted to those resulting from Tollmien–Schlichting type instabilities. On the other hand, material response alone is not an indicator of the ability of a particular coating to reduce the turbulent energy in the surrounding flow field. Before such data can be interpreted in terms of drag-reduction capabilities, the effects of amplitude, frequency, and phase response on instabilities or on the turbulent bursting phenomenon must be better understood. Among recent attempts to understand these effects are numerical studies that assume a certain response of a membrane or Voigt solid and couple this response back into the flow field. The "smart-wall" studies by McMurray and Metcalfe [20] and Riley *et al.* [21] have shown the ability of wall motion to transfer energy from higher to lower wavenumber modes. In earlier work Orszag [22] computed the velocity profile following a turbulent burst assuming a pressure pulse due to the burst. Results were shown to depend on the wavelength of the wall motion.

Recently attention has turned from the interaction of a coating with a fully developed turbulent boundary layer to the possibility of delaying transition of the boundary layer from laminar to turbulent. Indeed, Kramer believed that this delay was responsible for the drag reduction that he was able to achieve. Carpenter and Garrad [15] suggest that the failure of later experiments (those with coatings similar to Kramer's) to duplicate Kramer's results may be due to the unsuitability of these experiments for investigating transition. Using a model representing a modified potential flow over a single-layer isotropic Voigt material, Duncan, Waxman, and Tulin [23] derived analytically a dispersion relation for two-dimensional wavetrains on the interface. Although the purpose of their paper was to describe the effects of damping on wave propagation and to shed light on experimental results, they did conclude that the onset velocity for Tollmien–Schlichting instabilities, classified as class A instabilities by Benjamin [24], was higher for laminar boundary layers than for turbulent ones.

In this paper, we consider a numerical method for studying the interaction between a Tollmien–Schlichting wave and a variety of compliant coatings. A

pseudospectral solution of the incompressible Navier–Stokes equation is coupled through the boundary conditions to a finite element calculation of the response of a linear visco-elastic solid. The pseudospectral solution employed is a time-splitting method, with the compliant wall boundary conditions enforced during both the pressure and viscous steps. Since the method does not force conservation of mass, errors introduced in the near-wall region due to the time-splitting quickly become evident in calculation of the divergence. Iteration of both the pressure and viscous corrections, as described below, is used to minimize this error. We believe that this method can be useful in the study of flow over a greater variety of material configurations than can be easily modeled analytically

1. Initial Conditions

Transition will be delayed if the compliant coating can in effect raise the critical Reynolds number of the boundary layer flow. This corresponds to a shifting of the neutral stability curve of the Orr-Sommerfeld equation, describing the evolution of a small disturbance (a Tollmien–Schlichting wave) in the flow. The shift in the neutral stability curve due to a compliant coating was calculated analytically by Benjamin [25] using a single parameter, which he called the response coefficient, to represent the properties of the compliant material. Stability curves were calculated numerically by Landahl [26], Kaplan [27], and by Landahl and Kaplan [28] for a spring-backed membrane with damping. In addition to reproducing the results of Kaplan and Landahl and Kaplan, Garrad [29] and Carpenter and Garrad [15] have used this method to examine the stability properties of Kramer-type coatings. They modeled a Kramer-type surface as an elastic plate backed by a viscous fluid and supported by springs, which were in turn modeled by an elastic foundation (see also Ref. [30]). Their results indicate that there may indeed be Kramer-type coatings that are able to stabilize Tollmien–Schlichting instabilities that would grow in the presence of a rigid surface.

In this paper, we use as the initial condition for our calculations a Tollmien–Schlichting wave that is known to be unstable, super-imposed on a Blasius boundary layer. Initially, the interface between the fluid and the solid is flat, and the velocity on the interface is zero (Fig. 1). The growth rate of the wave is calculated over a certain length of time, and this growth rate, as well as the phase shift between the Tollmien–Schlichting wave and the resulting wave in the compliant coating, are examined and compared for a variety of materials. All of our calculations are done using a Reynolds number of 1000 based on the displacement thickness δ^*, where δ^* is equal to 1.72, and a Tollmien–Schlichting wave of wavenumber α equal to 0.225, where α has been made dimensionless by multiplying by δ^*. This wave represents the most unstable mode of the Orr–Sommerfeld equation for the given Reynolds number. In the presence of the rigid wall, the growth rate of the wave is calculated to be 0.0144 after 2000 time steps of 0.005 s. The growth rate predicted by linear theory is between 0.014 and 0.015 [15]. The

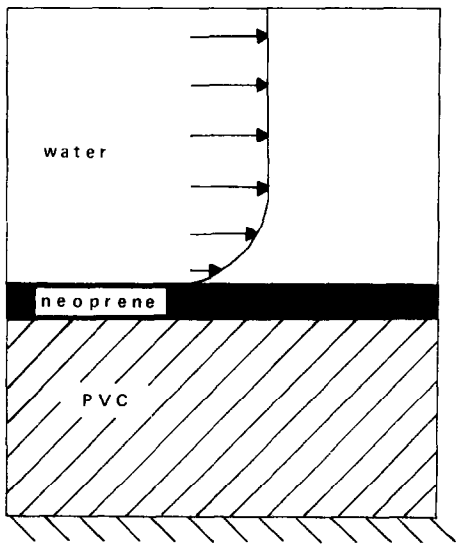

FIG 1 Coupled integration domain

initial velocity field in the fluid, consisting of the Tollmien–Schlichting wave and the underlying Blasius flow, is calculated using an Orr–Sommerfeld solver similar to that used by McMurray *et al.* [20] for their "smart-wall" calculations, done using the pseudospectral code originally developed by Orszag and Kells [31].

In the results that follow, we find that certain compliant materials do indeed have the capability of stabilizing the Tollmien–Schlichting wave. It should be noted, however, that the Tollmien–Schlichting type instability, which arises in the presence of a rigid surface as well as in the presence of a compliant surface, is one of three types of instabilities that arise in the presence of a compliant surface. These three instabilities were classified by Benjamin [24, 25] and consist of the Tollmien–Schlichting instability, which is destabilized by damping, a surface wave instability similar to that induced by wind over water, which is stabilized by damping, and the Kelvin–Helmholtz instability [26]. As Benjamin [25] points out, it might be useless to employ a compliant coating that inhibits one type of instability but not another. These results therefore represent only a part of the information that would be required before a decision could be made as to what the effect of a compliant coating would be on skin-friction drag.

2. Coupling of the Fluid and Solid Equations

The equations of motion for the flow field are the incompressible Navier–Stokes equation written in rotational form

$$\frac{\partial \mathbf{v}(\mathbf{x}, t)}{\partial t} = \mathbf{v}(\mathbf{x}, t) \times \boldsymbol{\omega}(\mathbf{x}, t) - \nabla \pi(\mathbf{x}, t) + \nu \nabla^2 \mathbf{v}(\mathbf{x}, t) \tag{2.1}$$

together with the continuity equation

$$\nabla \cdot \mathbf{v}(\mathbf{x}, t) = 0, \tag{2.2}$$

where $\mathbf{v}(\mathbf{x}, t) = (u, w)$, $\mathbf{x} = (x, z)$, $\boldsymbol{\omega}(\mathbf{x}, t) = \nabla \times \mathbf{v}(\mathbf{x}, t)$, $\pi(\mathbf{x}, t) = p(\mathbf{x}, t) + \frac{1}{2}|\mathbf{v}(\mathbf{x}, t)|^2$, and ν is the kinematic viscosity. Periodic boundary conditions are imposed in the streamwise direction, enabling us to express the velocity field as a truncated Fourier series in x. At the interface between the fluid and the solid, we impose a linearized Dirichlet boundary condition. This linearization restricts us to examining small displacements of the wall. Since the component of wall motion in the streamwise direction is very much smaller than that in the direction normal to the flow, a further simplification involves neglecting the advective term in the boundary condition. We will denote by η the displacement of the wall in the direction normal to the wall, and we will use the subscript fe to identify quantities calculated by the finite element code. Then, in particular, the true expression for w is given by

$$w = \frac{Dz}{Dt} = \frac{\partial \eta}{\partial t} + u_{\text{fe}} \frac{\partial \eta}{\partial x}; \tag{2.3}$$

however, for all of the materials tested, $u_{\text{fe}}(\partial \eta/\partial x) \ll \partial \eta/\partial t$, and the approximation $w = \partial \eta/\partial t$ is used. This inequality is graphically illustrated for neoprene over soft polyvinylchloride (PVC) in Fig. 2. To first order in the displacement η,

$$w(0, t) = w(\eta, t) - \eta \frac{\partial}{\partial \eta} w(0, t), \tag{2.4}$$

and linearizing, we set $w(0, t) = w(\eta, t)$

In the direction normal to the wall, the interval $(-1, 1)$ is mapped to $(0, 20)$, with about one-third of the Chebyshev collocation points located in the boundary layer. We will denote by $\mathbf{v}_{\text{fe}}$ the velocity calculated by the finite element code. Thus at time t, the boundary condition for the flow field is given by $\mathbf{v}(x, 0, t) = \mathbf{v}_{\text{fe}}(x, \eta, t)$. At $z = 20$, $\mathbf{v}(x, 20, t) = (U, 0)$, the freestream velocity.

The velocity is represented by

$$\mathbf{v}(\mathbf{x}, t) = \sum_{|m| < M} \sum_{p=0}^{P} \mathbf{u}(m, p, t) \exp[2\pi i m x/X]\, T_p(z), \tag{2.5}$$

where $T_p(z)$ is the Chebyshev polynomial of degree p, defined by $T_p(\cos\theta) = \cos p\theta$. We use 33 Chebyshev modes and 32 Fourier modes for all of our calculations.

The calculation proceeds by first allowing the flow field to develop for a short time Δt, during which a pressure history at the wall is generated. Numerical integration of the Navier–Stokes equation is accomplished in three fractional time steps. The nonlinear term $\mathbf{v} \times \boldsymbol{\omega}$ is calculated in physical space for the sake of computational efficiency. That is, $\mathbf{v}$ and $\boldsymbol{\omega}$ are obtained in spectral space and are then transformed to physical space, where the cross product is taken. The result is

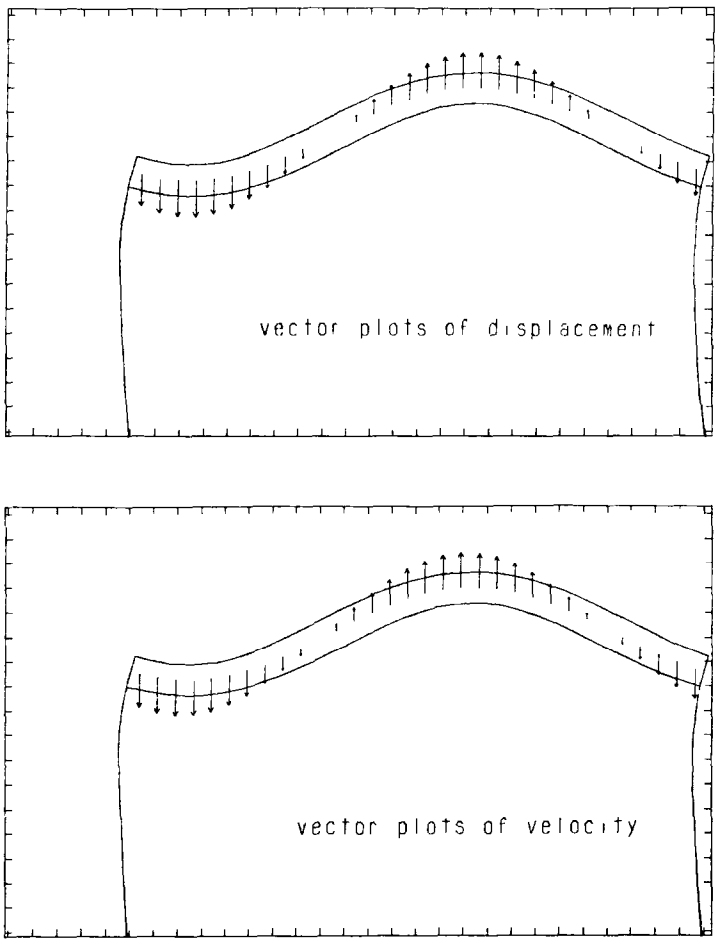

FIG 2 Vector plots of the displacement and velocity in neoprene over soft PVC

transformed back into spectral space, where all time stepping is performed. The first fractional time step is given by

$$\hat{\mathbf{v}}(t) = \mathbf{v}(t) - \int_t^{t+\Delta t} \mathbf{v} \times \boldsymbol{\omega}\, dt \tag{2.6}$$

and is performed explicitly using a second-order Adams–Bashforth method.

The second fractional time step is the addition of the pressure term

$$\hat{\hat{\mathbf{v}}}(t) = \hat{\mathbf{v}}(t) - \int_t^{t+\Delta t} \nabla \pi\, dt. \tag{2.7}$$

To obtain the pressure, we solve the Poisson equation

$$\nabla^2 p = \nabla \cdot (\mathbf{v} \times \boldsymbol{\omega}) - \tfrac{1}{2}\nabla^2(|\mathbf{v}|^2) \tag{2.8}$$

with periodic boundary conditions in the streamwise direction, and setting p equal to zero at $z = 20$. At the interface, we want

$$\nabla \pi = \frac{1}{\Delta t}\left[\hat{\mathbf{v}}(t) - \mathbf{v}_{\text{fe}}(t + \Delta t)\right] + \nu \nabla^2 \mathbf{v}(t + \Delta t). \tag{2.9}$$

We have, instead,

$$\nabla \pi = \frac{1}{\Delta t}\left[\hat{\mathbf{v}}(t) - \mathbf{v}_{\text{fe}}(t + \Delta t)\right] + \nu \nabla^2 \mathbf{v}(t) \tag{2.10}$$

and iteration through the pressure and viscous steps is performed at each time step. This results in an implicit pressure correction, after iteration. During the initial development of the flow field, $\mathbf{v}_{\text{fe}} = 0$. To avoid oscillation of the pressure in the z direction, and since the right-hand side of the Poisson equation is calculated in physical space, the equation is solved in physical space in the z direction and spectral space in x. Uneven grid points exactly match the Chebyshev collocation points to maintain resolution in the near wall region. The physical pressures are used as load curves to drive the compliant material.

The pressure head is transformed to spectral space to complete this fractional time step. The streamwise component of the velocity is found from the corresponding momentum equation

$$\hat{\hat{u}}(t) = \hat{u}(t) - \int_t^{t + \Delta t} \frac{\partial \pi}{\partial x}\, dt, \tag{2.11}$$

and the normal component from the continuity equation

$$\frac{\partial \hat{\hat{u}}(t)}{\partial x} + \frac{\partial \hat{\hat{w}}(t)}{\partial z} = 0. \tag{2.12}$$

Monitoring of the error in the divergence at each time step was used as a diagnostic tool in developing the code and during coupled calculations. An increase in this error near the wall supported the theory that the greatest error was incurred as a result of the use of a linearized boundary condition.

Finally, the viscous correction

$$\mathbf{v}(t + \Delta t) = \hat{\hat{\mathbf{v}}}(t) + \int_t^{t + \Delta t} \nu \nabla^2 \mathbf{v}\, dt \tag{2.13}$$

is done by a fully implicit spectral-tau method. The final velocity at the wall satisfies $\mathbf{v}(t + \Delta t) = \mathbf{v}_{\text{fe}}(t + \Delta t)$ in both the normal and tangential components.

The pressure history generated by the flow calculation is used to drive a compliant material for a corresponding length of time. Material response is calculated by DYNA2D, the two-dimensional version of the finite element code developed by Hallquist [32]. The equations of motion solved by DYNA2D are:

$$\frac{\partial \Sigma_{xx}}{\partial x}+\frac{\partial T_{xz}}{\partial z}=\rho \frac{\partial^2 x}{\partial t^2} \tag{2.14a}$$

$$\frac{\partial T_{xz}}{\partial x}+\frac{\partial \Sigma_{zz}}{\partial z}=\rho \frac{\partial^2 z}{\partial t^2} \tag{2.14b}$$

$$\Sigma_{xx}=S_{xx}-(P+q) \tag{2.14c}$$

$$\Sigma_{zz}=S_{zz}-(P+q), \tag{2.14d}$$

where Σ_{xx} and Σ_{zz} are the total stresses, T_{xz} is the shear stress, ρ is the density, and S_{xx} and S_{zz} are the stress deviators, which are determined by the visco-elastic model P is the hydrostatic pressure, and q is the artificial viscosity, given by

$$q=C^2\rho^0\left(\frac{1}{V}\frac{\partial V}{\partial t}\right)^2\frac{A}{V}. \tag{2.15}$$

Here, C is a constant, ρ^0 is the reference density, V is the volume, and A is the zone area. In addition to these equations we have the continuity equation

$$\frac{1}{V}\frac{\partial V}{\partial t}=\frac{\partial^2 x}{\partial x\,\partial t}+\frac{\partial^2 z}{\partial z\,\partial t}, \tag{2.16}$$

and the energy equation

$$\frac{\partial E}{\partial t}=-(P+q)\frac{\partial V}{\partial t}+V\left(S_{xx}\frac{\partial \varepsilon_{xx}}{\partial t}+S_{zz}\frac{\partial \varepsilon_{zz}}{\partial t}+T_{xz}\frac{\partial \varepsilon_{xz}}{\partial t}\right), \tag{2.17}$$

where the velocity strains are given by

$$\frac{\partial E_{xx}}{\partial t}=\frac{\partial^2 x}{\partial x\,\partial t},\qquad \frac{\partial \varepsilon_{zz}}{\partial t}=\frac{\partial^2 z}{\partial z\,\partial t};\qquad \frac{\partial \varepsilon_{xz}}{\partial t}=\frac{\partial^2 z}{\partial x\,\partial t}+\frac{\partial^2 x}{\partial z\,\partial t}. \tag{2.18}$$

The equation of state is

$$P=-k\ln V, \tag{2.19}$$

where k is the bulk modulus of the material.

For a linear visco-elastic material, input parameters to DYNA2D include the density, bulk modulus, short-time shear modulus G_0, long-time shear modulus G_∞, and the decay constant, β_{fe}. The last three parameters define the shear relaxation behavior as follows:

$$G(t)=G_\infty+(G_0-G_\infty)\,e^{-\beta_{fe}t}. \tag{2.20}$$

In our calculations, the bottom surface of the material is rigid, and the sides are constrained to move together, to provide the periodic interface velocities that are consistent with the fluid calculation. The pressure loading is applied at the interface, and water elements are placed above this interface to account for the mass of the water sitting over the material. A discussion of the effect of this added mass can be found in Reference [16]. The height of these elements is chosen so as to result in a free surface at the top that does not respond to material displacements.

The coupling algorithm begins, as stated above, with the fluid code marching from time zero to some time Δt, and writing a pressure history. A pressure loading curve is thus provided to drive the finite element code from $t=0$ to $t=\Delta t$ The finite element code now runs from zero to Δt, and calculates values of the velocity at nodal points on the interface at time Δt The explicit finite element code takes a time step that is smaller by approximately an order of magnitude than that taken by the fluid code. For this reason the finite element code sub-cycles within time Δt, and first-order interpolation is used to obtain the necessary boundary pressures. In using the velocities resulting from this calculation as a boundary condition for the pressure routine and for the spectral-tau viscous calculation, interface velocities are transformed to Fourier space. The fluid code now runs from $t=0$ to $t=2\Delta t$, with $\mathbf{v}=\mathbf{v}_{fe}$ at the interface at time Δt, and then from $t=\Delta t$ to $t=2\Delta t$ with, as an initial estimate, $\mathbf{v}$ at the interface decaying smoothly A pressure history is written for the interval $\Delta t \leqslant t \leqslant 2\Delta t$, which drives the solid during the subsequent finite element calculation. Coupling of the two codes proceeds with iteration of the flow calculation over each time interval.

This marching scheme is algorithmically equivalent to one code solving the appropriate equations in two connected blocks of mesh. Block one consists of the fluid, and as a first approximation the interface is assumed to be flat. Block two, the solid, is then given boundary data resulting from the calculation in block one, and the solid equations are solved over the same time interval. The code then repeats calculation of the first block, with the new interface velocities as corrected data. After this, the code restarts at time Δt, with smoothly decaying velocities as the first approximation of the interface boundary condition for the interval $\Delta t \leqslant t \leqslant 2\Delta t$.

To summarize some of the features of the numerical method, the flow field is represented by a truncated Fourier series in x and a truncated Chebyshev series in z. A pseudospectral method is used to calculate the nonlinear and pressure terms, and a spectral-tau method is used for the viscous correction. The pressure calculation is done by finite difference, with the unevenly spaced grid retaining the boundary layer resolution obtained by using a Chebyshev expansion in z. The calculations presented below were done using 32 modes in x ($M=16$) and 33 modes in z ($P=32$). The fluid code requires about 1 5 ms per mode per time step on a CRAY-1 computer.

The finite element calculation is formally second-order accurate both spatially and temporally. Typical calculations were done using 256 four-node elements, requiring 297 nodal points. The code runs in about 17 ms per nodal point per time step on a CRAY-1 computer.

3. Results

The first material examined with the coupled calculation was a 2.5 cm thick layer of a soft polyvinylchloride (PVC). This nearly incompressible gelatinous material was used in the noninteractive numerical calculation of material response done by Buckingham *et al.* [16], and in the experimental study of surface instability done by Gad-el-Hak [11]. The material parameters required by the DYNA2D code were the material density, the bulk modulus, the short and long term shear moduli G_0 and G_∞, and the decay constant, β. Table I lists these values for this and other materials used in our calculations. The shear modulus $G(t)$ of the material is modeled by

$$G(t) = G_\infty + (G_0 - G_\infty)\, e^{-\beta t}. \tag{3.1}$$

After ten coupled time intervals, a footprint of the Tollmien–Schlichting wave can be seen in the polyvinylchloride. The displacements from the initial state are shown in Fig. 3. These displacements are scaled by a factor of fifty to make the wave clearly visible. The ratio of the actual amplitude of the displacement to the wavelength is approximately 0.001, and is small enough both to ensure that the flow will not separate and to make the use of linearized boundary conditions in the fluid calculation feasible (cf. Benjamin [33] and Miles [34]). The displacements are not scaled in Fig. 4, which shows the actual configuration of the PVC after 40 coupled time intervals. Displacements in the PVC are now great enough to cause separation of the flow from the surface and order-one error in the solution of the Navier–Stokes equation due to the boundary conditions, and the calculation was stopped at this point. This displacement corresponds to an increase in the energy contained in the Tollmien–Schlichting wave equal to two orders of magnitude and, at the final time, the growth rate of the disturbance is 90 times the growth rate in the presence of the rigid wall. The grid is being advected along with the Tollmien–Schlichting wave, and a phase lag of approximately one tenth of a wavelength is noticeable in this soft material. The phase shift seen here can be interpreted as a "quasi-sheltering" of the wave, using the terminology of Benjamin [33], where by "sheltered," it is implied that the pressure is lower on the leeward side of

TABLE I

Material Parameters Used in Finite Element Calculation of Material Response

	Soft PVC	Stiff PVC	Neoprene
Density (kg/m^3)	1025	1025	1320
Bulk Modulus (Pa)	7.75×10^7	7.75×10^7	3.43×10^9
Short time shear modulus (Pa)	24.3	2.74×10^4	9.76×10^6
Long time shear modulus (Pa)	7.70	1.0×10^4	3.50×10^6
Decay constant (s^{-1})	600	120	135

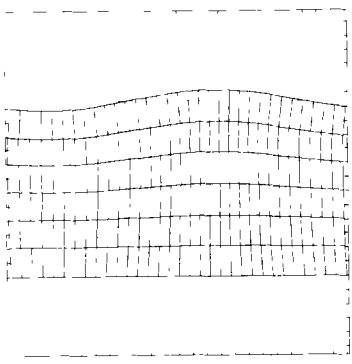

FIG 3 Response of the soft polyvinylchloride to pressures induced on the surface by the Tollmien–Schlichting wave, after ten coupled time intervals The displacements are scaled by a factor of fifty The broken line indicates the original location of the undisturbed interface

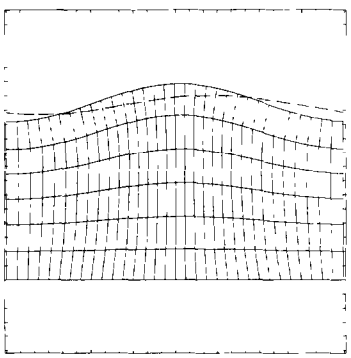

FIG 4 The actual shape of the soft PVC after 40 coupled time intervals The broken line indicates the initial footprint of the Tollmien–Schlichting wave, as is illustrated in Fig 3

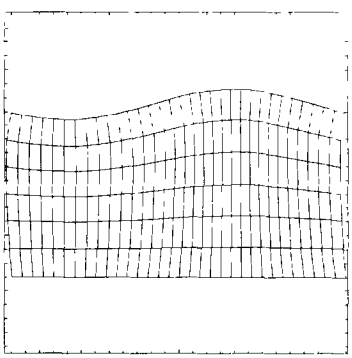

FIG 5 The shape of the stiff PVC after 40 coupled time intervals The displacements are scaled by a factor of 2000

the wave due to separation of the flow from the surface [35, 36]. Quasi-sheltering occurs when there is no separation of the flow [37]. The highly unstable response of this soft PVC prevented further calculation.

We next performed the same calculation using 2.5 cm of a stiffer polyvinylchloride. After ten coupled time intervals, we again see a footprint of the fluctuation in the solid. However, the amplitude of the displacement is roughly 5% of that seen in the softer material. After 40 coupled time intervals, comparison of the displacement in the solid with that in the softer material shows that the disturbance has attained only 0.05% of the amplitude obtained by the soft PVC. The displacement is scaled by a factor of two thousand in Fig. 5. The wave in the surface, rather than lagging behind the disturbance in the flow field, is seen to be somewhat downstream of it, with the phase shift being equal to approximately one-twelfth of the wavelength. In Fig. 6, we have superimposed Fig. 5 on the initial footprint of the Tollmien–Schlichting wave (Fig. 3) to illustrate this phase difference. As the calculation continues, the wave gradually slows in both phase shift and growth. The calculation was stopped after one hundred coupled intervals, at which time the wave amplitude and the phase shift have stablized. Figure 7 depicts the final state attained by the stiff PVC. The displacements are scaled by a factor of one thousand.

The final material tested was a 2.5 cm thick layer of soft PVC covered by a 0.25 cm layer of rubber-like neoprene. We again see a footprint of the Tollmien–Schlichting wave in the material after ten coupled intervals. The displacement, while roughly an order of magnitude smaller than that in the soft PVC alone, is twice as great as that in the stiffer material. This material configuration was chosen after the uncoupled numerical study of Buckingham *et al.* [16] suggested that the combination of neoprene over PVC might be a promising candidate for reducing drag. This suggestion was based on an examination of the amplitude and frequency response of the material to random pressure fluctuations modeling a turbulent flow. However, our coupled results indicate that the material permits rapid growth of the Tollmien–Schlichting instability, indicating that the boundary layer is linearly unstable at lower Reynolds numbers than for the case of a rigid wall. In Fig. 8, displacements are scaled by a factor of ten. Comparing this with Fig 4, in which displacements are not scaled, shows that while the amplitude of the disturbance remains an order of magnitude smaller than that seen in the soft PVC alone, the added neoprene has had no effect on the phase lag. Possibly as a consequence, after 40 coupled time steps, the growth rate of the Tollmien–Schlichting wave is again 90 times that of the wave in the presence of a rigid wall.

To summarize our results, three coatings were tested in this study; a 2.5 cm thick layer of soft polyvinylchloride (PVC), a layer of a stiffer PVC of the same thickness, and a 2.5 cm thick layer of soft PVC covered by a 0.25 cm layer of neoprene. The unforced response of these materials to surface pressure was calculated, with particular attention being paid to phase shift, amplitude, and growth rate of the resulting disturbance. In turn, the effect of material response on the flow field in which the disturbance originated was examined All flow calculations were done at a Reynolds number based on a displacement thickness of 1000. The wave in the soft

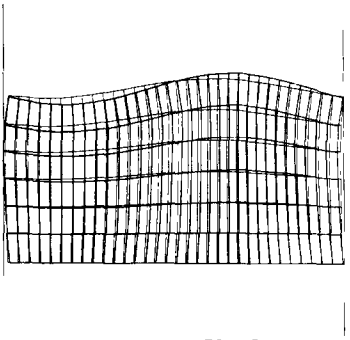

FIG 6 Figure 5 superimposed on the initial footprint of the Tollmien–Schlichting wave, showing the phase shift in the material disturbance after 40 coupled time intervals

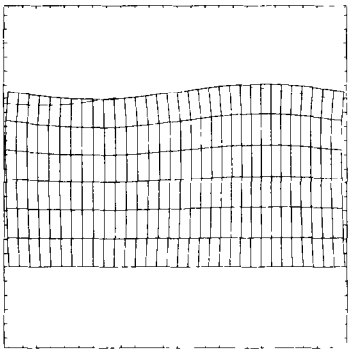

FIG 7 The final state attained by the stiff polyvinylchloride before coupling was discontinued Displacements are scaled by a factor of 1000 The broken line indicates the initial footprint of the Tollmien–Schlichting wave

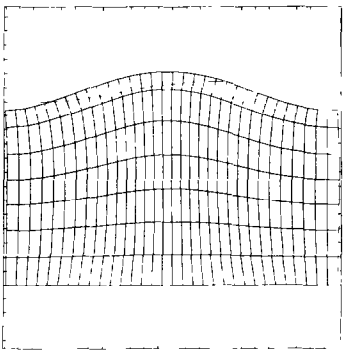

FIG 8 Soft PVC, covered by a thin layer of neoprene after 40 coupled time steps Displacements are scaled by a factor of 10 The broken line indicates the initial footprint of the Tollmien–Schlichting wave

PVC that resulted from a single Tollmien–Schlichting wave superimposed on a boundary layer flow profile was seen to lag behind the wave in the flow. After 40 coupled time steps, the disturbance was growing rapidly, and the calculation was discontinued when the linearized boundary condition was no longer adequate. Coating this material with a thin layer of neoprene controlled the amplitude of the response but had no effect on the phase lag. After 40 coupled time steps, the wave was again seen to be growing rapidly. The firm PVC, on the other hand, developed a wave that was shifted slightly downstream of the Tollmien–Schlichting wave and attained a steady state.

Acknowledgment

I thank Alfred C Buckingham for his friendship, support, encouragement, and helpful discussions throughout the time spent on this work I also thank Michael M Reischman at the Office of Naval Research, Lewis A Glenn at LLNL, and John O Hallquist at LLNL for support and helpful discussions

References

1 M O Kramer, *New Sci* **7**, 1118 (1960)
2 M O Kramer, *Adv Hydrosci* **2**, 111 (1965)
3 M O Kramer, *J Aero Sci* **24**, 459 (1957)
4 M O Kramer, *J Amer Soc. Naval Eng* **72**, 25 (1960), *J Aero/Space Sci* **27**, 69 (1960)
5 M O Kramer, *J Amer Soc Naval Eng* **74**, 341 (1962)
6 C R Nisewanger, U S Naval Ordnance Test Station, China Lake, Report No NAVWEPS Rep 8518, 1964 (unpublished)
7 F W Puryear, U S Dept of Navy, David Taylor Model Basin Report 1668, 1962 (unpublished)
8. H Ritter and L T Messum, Admiralty Research Laboratory Report ARL/G/N9, 1964 (unpublished)
9 H Ritter and J S Porteous, Admiralty Research Laboratory Report ARL/N3/G/HY/9/7, 1965 (unpublished)
10 D M Bushnell, J N Hefner, and R L Ash, *Phys Fluids* **20**, 531 (1977)
11 M Gad-el-Hak, R F Blackwelder, and J J Riley, *J Fluid Mech* **140**, 257 (1984)
12 M Gad-el-Hak, R F Blackwelder, and J J Riley, "Interaction of Compliant Surfaces with Transitional and Turbulent Boundary Layers," *Structure of Complex Turbulent Shear Flow*, edited by R. Dumas and L Fulachier, (Springer-Verlag, Berlin, 1982), p 20
13 P B S Lissaman and G L Harris, "Turbulent Skin Friction on Compliant Surfaces," AIAA 7th Aerospace Sciences Meeting, New York, 1969
14 J M McMichael, P S Klebanoff, and N E Mease, "Experimental Investigation of Drag on a Compliant Surface," *Viscous Flow Drag Reduction*, edited by G R Hough, Progress in Astronautics and Aeronautics Vol 72 (AIAA, New York, 1980), p 410
15 P W Carpenter and A D Garrad, *J Fluid Mech* **155**, 465 (1985)
16 A C Buckingham, M S Hall, and R C Chiu, *AIAA J* **23**, 1046 (1985)
17 R L Ash, National Aeronautics and Space Administration Report No NASA CR-2958, 1978 (unpublished)
18 R L Ash and M Khorrami, "Simulation of Turbulent Wall Pressure Fluctuations for Flexible Surface Response Studies," AIAA 21st Aerospace Sciences Meeting, Nevada, 1983
19 O M Phillips, *J Fluid Mech* **2** 417 (1957)

20 J T McMURRAY AND R W METCALFE, Flow Research Company, Kent, WA, private communication (1983)
21 J J RILEY, C RUTLAND, AND R W METCALFE, "The Stabilization of Inviscid Instabilities in a Temporally Growing Boundary Layer by Wall Forcing," American Physical Society Division of Fluid Dynamics 37th Annual Meeting, Providence, RI, 1984
22 S A ORSZAG, National Aeronautics and Space Administration Report No NASA CR-3071, 1979 (unpublished)
23 J H DUNCAN, A M WAXMAN, AND M P TULIN, *J Fluid Mech* **158**, 177 (1985)
24 T B BENJAMIN, *J Fluid Mech* **16**, 436 (1963)
25 T B BENJAMIN, *J Fluid Mech* **9**, 513 (1960)
26 M T LANDAHL, *J Fluid Mech* **13**, 609 (1962)
27 R E KAPLAN, Sc D Thesis, MIT, 1964 (unpublished)
28 M T LANDAHL AND R E KAPLAN, AGARDograph 97-1-353, 1965
29 A D GARRAD, Ph D thesis, University of Exeter, 1980 (unpublished)
30 P W CARPENTER, M. GASTER AND G J K WILLIS, "A Numerical Investigation into Boundary-layer Stability on Compliant Surfaces," *Numerical Methods in Laminar and Turbulent Flow*, edited by C Taylor *et al* (Pineridge, Swansea, 1983), p 166
31 S A ORSZAG AND L C KELLS, *J. Fluid Mech* **96**, 159 (1980)
32 J O HALLQUIST, Lawrence Livermore National Laboratory Report No. UCID-18756, 1982 (unpublished)
33 T B BENJAMIN, *J Fluid Mech* **6**, 161 (1959)
34 J W MILES, *J. Fluid Mech* **6**, 568 (1959)
35 H JEFFREYS, *Proc R Soc London A* **107**, 189 (1925)
36 H JEFFREYS, *Proc R Soc London A* **110**, 241 (1925)
37 J W MILES, *J Fluid Mech* **3**, 185 (1957)